

Spatiotemporal heterogeneity of local free volumes in highly supercooled liquid

Hayato Shiba*

Institute for Solid State Physics, University of Tokyo, Chiba 277-8581, Japan

Takeshi Kawasaki

Department of Physics, Kyoto University, Kyoto 606-8502, Japan[†]

(Dated: November 16, 2018)

We discuss the spatiotemporal behavior of local density and its relation to dynamical heterogeneity in a highly supercooled liquid by using molecular dynamics simulations of a binary mixture with different particle sizes in two dimensions. To trace voids heterogeneously existing with lower local densities, which move along with the structural relaxation, we employ the minimum local density for each particle in a time window whose width is set along with the structural relaxation time. Particles subject to free volumes correspond well to the configuration rearranging region of dynamical heterogeneity. While the correlation length for dynamical heterogeneity grows with temperature decrease, no growth in the correlation length of heterogeneity in the minimum local density distribution takes place. A comparison of these results with those of normal mode analysis reveals that superpositions of lower-frequency soft modes extending over the free volumes exhibit spatial correlation with the broken bonds. This observation suggests a possibility that long-ranged vibration modes facilitate the interactions between fragile regions represented by free volumes, to induce dynamical correlations at a large scale.

PACS numbers: 64.70.kj, 81.05.Kf, 61.43.Fs

I. INTRODUCTION

The reason for the drastic slowdown in dynamics when liquids are cooled toward the glass transition temperature has been a long-standing problem. In the last two decades, numerous efforts have been made to study this problem via molecular dynamics (MD) simulations.¹ The recently proposed concept of “dynamic heterogeneity”^{2–10} has indicated that there could be a contrast between the mobile and immobile regions of supercooled liquids on a large scale, as if there were critical fluctuations hidden behind the disordered configuration. Over the past several decades, suggestions have been made regarding the static origin of the cooperative rearranging region.^{11,12} In recent literature, considerable attention has been focused on the relation of dynamical heterogeneity to the structural heterogeneity of medium length-scale crystalline order,^{13,14} icosahedral order,^{15,16} local potential energy,¹⁷ and so on. There are also continuing discussions about whether or not growing length scales of structures occur in the vitrified states.^{18,19}

Density fluctuation is one of the candidate origins for such a static entity. In the context of certain experiments, particularly on metallic, polymer, and colloidal glasses, density fluctuations have been observed over small-to-large length scales.^{20–24} One of the primary theoretical challenges thus far has been the construction of statistical descriptions of solids and glasses including the effects of vacancies or local free volume.^{25–31} In MD simulations of binary mixtures usually employed in studies of supercooled liquids, density fluctuations are too weak to be captured clearly,^{3,14,32} and the correlation of such fluctuations to dynamical heterogeneity has only partially been observed.³³ In crystals subject to homogeneous melting,

wherein the density fluctuation is more pronounced than in glass, diffusion of interstitial defects with relatively smaller local densities is ascribed as the cause of cooperative motion in two³⁴ and three^{35,36} dimensions. By considering how similar the dynamical properties are in ordered and disordered systems, the role of density fluctuation in dynamical heterogeneity can be revealed much more clearly.

In spite of difficulties in studying the local density fluctuations, one method has recently enabled the possibility of capturing the “inherent structure” as a localized soft mode, which can be calculated from a static configuration of particles in a supercooled liquid with the use of normal mode analysis.^{37,38} Since this approach is, to our knowledge, the only established approach to predict tendencies of heterogeneity of dynamic propensity from a momentary configuration of the particles, it can be the bridge between dynamical heterogeneity and its origin. In this study, we examine the heterogeneities of the local density distributions and dynamics by capturing and tracing weakly existing density fluctuations in a constructive manner, and subsequently, we investigate its relationship to the inherent structure to clarify the probable role of the density fluctuation in dynamical heterogeneity. The composition of this paper is as follows: In Sec. II, the simulation model and methods are provided. The numerical analysis of the local density fluctuation and its heterogeneity is described in Secs. III A–C. In Sec. III D, the result is compared with the heterogeneity of normal modes. In Sec. IV concludes the paper.

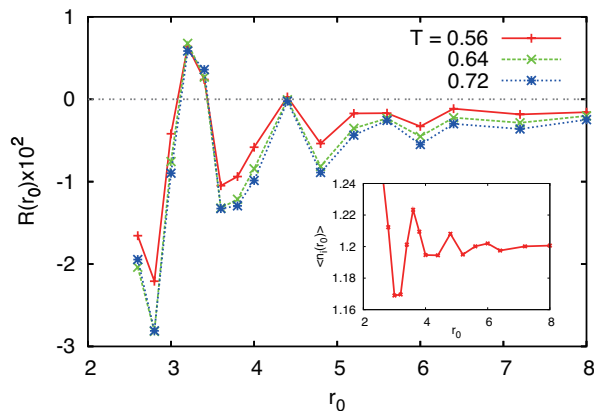


FIG. 1: Degree of deviation $R(r_0)$ of the local densities around the broken bonds $[n_i(r_0)]_{\text{b.b.}}$ (obtained at intervals of $\Delta t = 2 \times 10^2$) from that averaged over the entire system $[n_i(r_0)]_N$, plotted as a function of the averaging radius r_0 . The data for $T = 0.56, 0.64$, and 0.72 are shown. Inset: $\langle n_i(r_0) \rangle$ is shown for $T = 0.56$.

II. NUMERICAL METHOD

We investigate a two-dimensional (2D) binary mixture composed of two atomic species, 1 and 2, with $N_1 = N_2 = 32000$ particles. The particles interact via the soft-core potentials $v_{\alpha\beta}(r) = \epsilon(\sigma_{\alpha\beta}/r)^{12} + C_{\alpha\beta}$ where $\sigma_{\alpha\beta} = (\sigma_\alpha + \sigma_\beta)/2$ and r denote the interaction lengths and the distance between two particles respectively, with $\alpha, \beta \in \{1, 2\}$. The interaction is truncated at $r = 4.5\sigma_1$ and a constant $C_{\alpha\beta}$ is set so as to ensure continuity of the potential at the cutoff. The size ratio between the two species is $\sigma_2/\sigma_1 = 1.4$ to prevent crystallization, and the mass is set as $m_2/m_1 = (\sigma_2/\sigma_1)^2$. The particle density is fixed at a high value of $\phi = (N_1\sigma_1^2 + N_2\sigma_2^2)/V = 1.2$, and therefore the particle configurations are jammed in the supercooled state. No tendency of phase separation is detected in our computation times. Space, time, and temperature are measured in units of σ_1 , $\tau_0 = \sqrt{m_1\sigma_1^2/\epsilon}$, and ϵ/k_B , respectively. The dependence of the α -relaxation time on the temperature T is shown in Table I. A sufficiently long annealing time t_A is chosen ($t_A > 30\tau_\alpha$) with the time step being $\Delta t = 0.005$. The aging effect was negligible in the course of calculation of pressure, density time correlations, etc. After performing the above procedure at each temperature, we begin to collect the data. This time point in each of our simulations is denoted as $t = 0$ in the following.

III. RESULTS

A. Local density

First, for each particle i , we define the local density by counting the particles within the distance $\Delta r = |\mathbf{r} - \mathbf{r}_i| \leq$

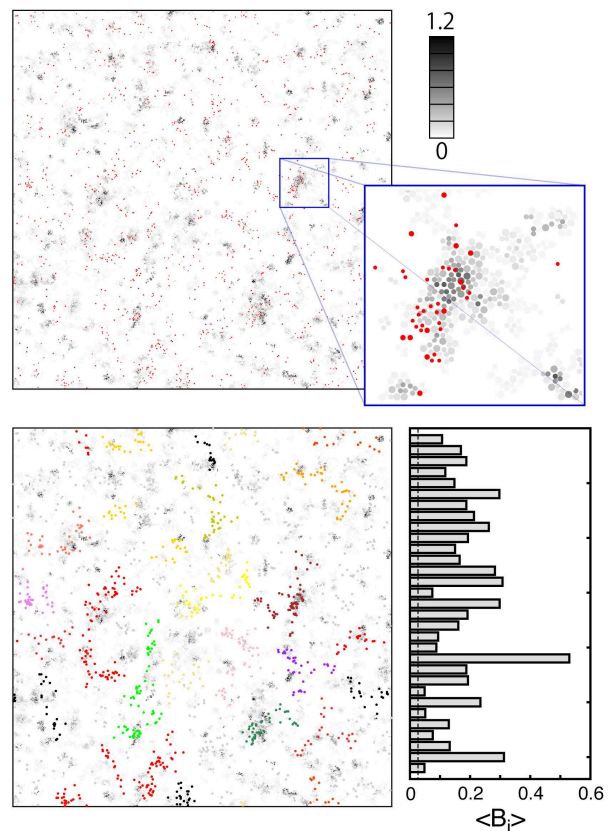


FIG. 2: (Top panel) The red points show the distribution of 2% of the particles having smaller local densities $\langle n_i(r_0) \rangle_{\text{IE}}$, which is averaged over $t \in [0, 10]$, in an IE of 32 runs at $T = 0.56$. The number distribution of broken bonds for the same IE $\langle \hat{B}(\mathbf{r}, \Delta t) \rangle_{\text{IE}}$ with $t \in [0, 122]$ is shown according to the scale bar on the right. For clarity, a magnified figure is shown to the right. (Bottom panel) In the left, for the same particle configuration as in the top panel, the particles are classified into several groups according to how they are close to each other. Each group is colored by a different color. To the right, the average value of the broken bond density $\langle B_i \rangle_{\text{IE}}$ over each cluster region is shown, where the dotted line indicates the average broken bond density $B_0 = 0.0268$.

r_0 from i

$$n_i(r_0) = \frac{1}{\pi r_0^2} \int_{\Delta r < r_0} d\mathbf{r} \sigma_j^2 \delta(\mathbf{r}_j - \mathbf{r}). \quad (1)$$

This local density is weighted by the assumed area σ_j^2 . The inset of Fig. 1 shows the long-time average of the local density $[n_i(r_0)]_N$ at $T = 0.56$. Here, $[\mathcal{A}_i]_N = N^{-1} \sum_i \mathcal{A}_i$ denotes the average over all the particles. This quantity corresponds to a radial distribution function $g(r_0)$ defined in a naive manner.

For the same simulation run, at appropriate time intervals, we estimate the local density in the configuration rearranging regions of dynamical heterogeneity as follows: bonds are defined at each time t_0 as particle

TABLE I: Dependence of α -relaxation time (τ_α) and bond-relaxation time (τ_b) on T .

T	0.56	0.64	0.72	0.80	0.96	1.20
τ_α	2.14×10^3	75.5	10.5	5.39	2.86	1.47
τ_b	1.41×10^5	1.90×10^4	5.25×10^3	1.87×10^3	5.35×10^2	1.85×10^2

pairs between i and j satisfying the condition^{2,3,8}

$$r_{ij}(t_0) \leq A_1 \sigma_{\alpha\beta} \quad (2)$$

and after a time interval Δt bonds are regarded to be broken if

$$r_{ij}(t_0 + \Delta t) > A_2 \sigma_{\alpha\beta}, \quad (3)$$

where the cutoffs are set to $A_1 = 1.15$ and $A_2 = 1.6$. Further, in the remainder of this paper, broken bonds in the time interval $[t, t + \Delta t]$ are defined in the same way. We obtain the local density profile only for particles that have undergone bond breakage in a time interval of $\Delta t = 2 \times 10^2$. More precisely, we check whether all the bonds existing at time $t = t_0$ are broken after a time interval of Δt , and for the particles having at least one broken bond the long-time average of the local density n_i is calculated. Their average local density profile is denoted as $[n_i(r_0)]_{\text{b.b.}}$. The main graph in Fig. 1 shows the long-time average $\overline{R}(r_0, \Delta t)$ of the relative degree of deviation as given by

$$R(r_0, \Delta t) = \left(\frac{[n_i(r_0)]_{\text{b.b.}}}{[n_i(r_0)]_N} - 1 \right). \quad (4)$$

While $R(r_0)$ exhibits an oscillating behavior at small values of r_0 mainly due to the mixed contributions from larger and smaller components, its value is systematically lower than zero when r_0 is sufficiently large. Thus, around the broken bonds, *i.e.*, in the configuration rearranging regions, the degree of local density can be characterized with a sufficiently large value of r_0 at each particle. We employ $r_0 = 6.0$ in our following discussions.

B. Broken bond and local free volume

Dynamic heterogeneity is defined as a ubiquitous property of supercooled liquids in which configuration-rearranging regions emerge heterogeneously in the system. This property can be parametrized with various quantities including the van Hove correlation,⁵ particle displacements,^{4,39} and four-point correlation functions. Here, to characterize the mobile regions of dynamical heterogeneity, we follow the method of broken bonds^{2,3,8}, in which the number of broken-bond pairs for each particle is counted as $\mathcal{B}_i(\Delta t) = \sum_{j \in \text{b.b.}} 1$. Here, the summation is taken over j particles at the broken bond ends of i particles calculated over time intervals of length Δt , where the definition of broken bond pairs is given by Eqs. (2)

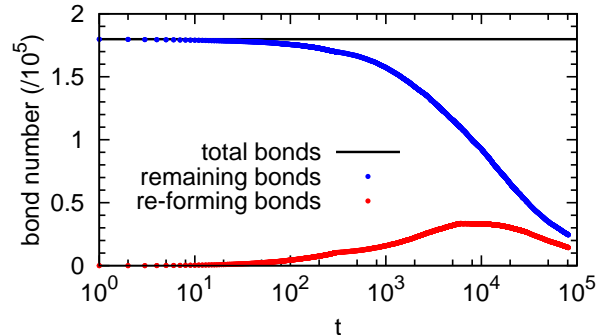


FIG. 3: Time development of the bond number for $T = 0.64$. The black line indicates the total number of the initial bonds, and the bonds are defined as pairs satisfying $r_{ij} < A_1 \sigma_{\alpha\beta}$ at $t = 0$. The blue points indicate the number of remaining bonds at time t . “re-forming bonds”, which denote those bonds that have undergone bond breakage and rebonding rebounded in a time interval of $[0, t)$, are indicated by the red points.

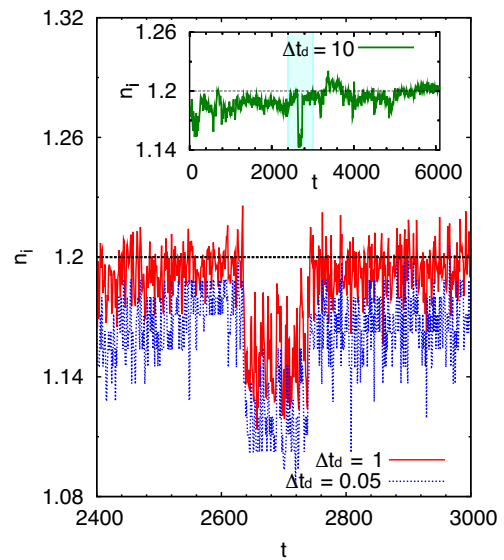


FIG. 4: Comparison of $n_i(r_0)$ and its minimum per every unit time. The red solid line shows the local density $n_i(r_0)$ ($r_0 = 6.0\sigma_1$) averaged over every unit time ($\Delta t_d = 1$) for a run at $T = 0.56$. On the blue dashed line, $n_i(r_0)$ is calculated for every time interval of $\Delta t_d = 0.05$ and each minimum is plotted per unit time. Therefore, the latter is systematically lower than the former due to thermal fluctuations on a small time scale. Inset: For the same particle and for a longer time interval, $n_i(r_0)$ is plotted when averaged over a time interval of $\Delta t_d = 10$.

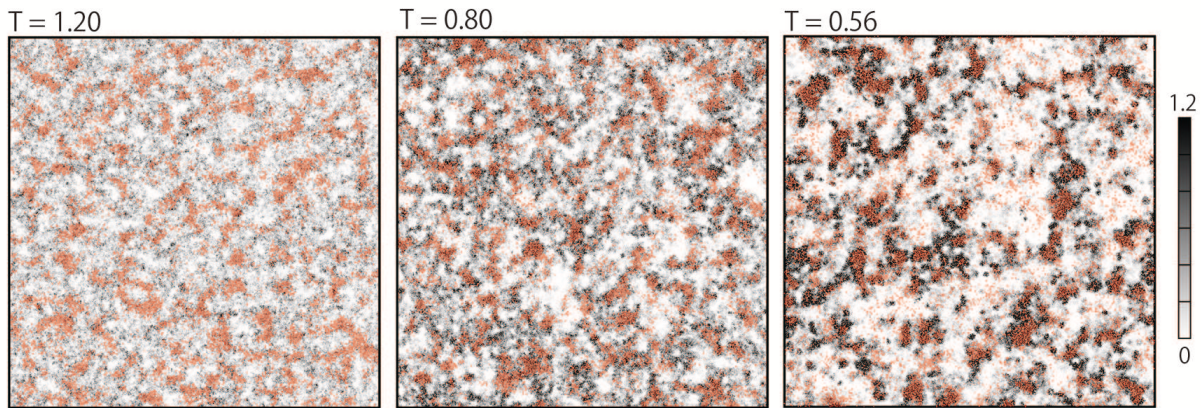


FIG. 5: The red points show the distribution of 25% of the particles having smaller values of minimum local densities $\langle \nu_i(\Delta t_b) \rangle_{\text{IE}}$, in an IE of 32 runs performed for $\Delta t_b = 6, 60,$ and 6100 for $T = 1.2, 0.80,$ and $0.56,$ respectively. The number distribution of broken bonds $\langle \mathcal{B}_i(\Delta t_b) \rangle_{\text{IE}}$ is shown by the gray scale according to the scale bar on the right.

and (3). The broken bond distribution is a representation of irreversible configuration rearrangements, where collective motion due to long-wavelength sound modes is eliminated. To illustrate the irreversibility of the bond breakage, in Fig. 3, the total number of the remaining bonds $N_b(t)$ ⁸ is plotted for $T = 0.64$, which is the number of unbroken bonds for the same thresholds A_1 and A_2 . Several pairs of particles i, j satisfying Eq. (2) at time $t = 0$ approach their counterparts again at time t' after themselves undergoing breakage. The number of these “re-forming bonds” is also shown in Fig. 3, where all the bond change is analyzed at every unit time. Because there are virtually no re-forming bonds at short time scales ($t \sim 10^2$), these bonds are not re-forming due to the vibration motion of the sound modes but because of the successive particle rearrangements or cage jump events. A particle pair is likely to remain separated with a probability of 80% once it becomes broken. As a result, the time-scale of local diffusion around these breaking bonds is characterized uniquely by bond-breakage relaxation time τ_b .^{8,40} Thus, broken bond characterizes a more qualified aspect of dynamical heterogeneity.

Since the spatial variation of dynamical heterogeneity strongly depends on the particle positions, isoconfigurational ensembles (IEs)^{41,42} of 32 runs are employed and an average is calculated over these runs. This IE average is denoted as $\langle \cdot \rangle_{\text{IE}}$ in the following discussions. In the top section of Fig. 2, we plot the $\langle \mathcal{B}_i(\Delta t) \rangle_{\text{IE}}$ values for a short time interval, $t \in [0, \Delta t]$ ($\Delta t = 122$), together with the distribution of 2% of particles having the lowest local densities $\langle n_i(r_0) \rangle_{\text{IE}}$ taken at the initial stage $t \in [0, 10]$. For $T = 0.56$, this lapse of time $\Delta t = 122$ is taken at a bit longer time than the typical lifetime of the voids (see Fig. 4), and thus, it corresponds to the time scale at initial stage of heterogeneous diffusion in the supercooled liquid. The particles with low local densities can be divided into heterogeneous clusters by grouping particles separated by distances shorter than 9σ into one cluster. These clus-

ters are depicted by differently colored particles in the bottom section of Fig. 2. We can see that these clusters have length scales exceeding 10σ , which means that there are several numbers of free volumes within each cluster existing heterogeneously in the supercooled state. These clusters are spatially correlated with configuration rearrangements whose degree is represented by a variable $\langle \hat{\mathcal{B}}(\mathbf{r}, \Delta t) \rangle_{\text{IE}}$, with $\hat{\mathcal{B}}(\mathbf{r}, \Delta t) = \sum_j \sigma_j^2 \mathcal{B}_j(\Delta t) \delta(\mathbf{r} - \mathbf{r}_j(0))$.⁸ In the bottom right part of Fig. 2 which shows the average value $\langle \mathcal{B}_i \rangle_{\text{IE}}$ for each of these clusters, we can see that all of these cluster values largely exceed the total average value $\mathcal{B}_0 = 0.0268$. It is also noteworthy that the larger clusters of free volumes shown in Fig. 2 as defined for instantaneous time ($\Delta t = 10$) are spatially correlated well with long-time dynamics as shown for $T = 0.56$ in Fig. 5.

To understand the cluster relationship with dynamical heterogeneity, it is necessary to understand how the clusters move over longer time intervals. For $T = 0.56, 0.64, 0.72, 0.80, 0.96,$ and 1.20 , simulation runs of IEs are performed with time intervals of $\Delta t_b(T) = 6100, 815, 210, 80, 23,$ and $8,$ respectively. Upon using the concept of bond relaxation time $\tau_b(T)$ introduced in a previous study³ and defined by the relation $N_b(t_0 + \tau_b) = N_b(t_0)/e$, these time intervals satisfy $\Delta t_b(T) \simeq 0.043\tau_b(T)$. Here, $N_b(t)$ denotes the total number of initial bonds ($t = 0$) remaining at time t , and $\tau_b(T)$ characterizes the time scale of structural relaxation (see Table I for actual values). In these intervals, almost identical portions of the total initial bonds undergo breakage for all values of T .

For low T values, wherein the system is dominated by slow dynamics, particle rearrangements agitated by thermal fluctuations are expected to become intermittent. In Fig. 4, for $T = 0.56$, the change in the local density n_i with time is measured for one specific particle in the mobile region of dynamical heterogeneity. By taking the average of n_i over every time interval of $\Delta t_d = 10$

as shown in the inset, the local density is observed to fluctuate around ϕ . In the region around $t = 2700$, the density reduces for a time interval of order 10^2 by an amount of around $\Delta n_i \simeq 0.05$. Interestingly, since $\Delta n_i \times \pi(r_0/2)^2 \sim O(1)$, this reduction corresponds to a free volume size of the scale of one particle, for the current radius $r_0 = 6.0$. The lower the temperature is, the longer the time interval is expected to be due to smaller thermal fluctuations. Upon decreasing the averaging time Δt_d to 1 and 0.05, the temporal fluctuation of $n_i(r_0)$ appears more explicitly. In the main graph, the red solid line represents $n_i(r_0)$ averaged over $\Delta t_d = 1$. For a considerably shorter time interval of $\Delta t_d = 0.05$, we accumulate the data of the density, and for every interval of unit time length ($\Delta t = 1$), we take the minimum of $n_i(r_0)$. The blue dashed line represents the minimum value of the local density for each unit time thus taken. Because these two lines follow parallel trajectories for low values of the density the minimum value in the local density history assumed by one particle can well represent and characterize the general time development of the local density.

C. Heterogeneity of local density

Since the heterogeneity of free volumes shown in Fig. 2 is very weak, we define the “minimum local density”

$$\nu_i(\Delta t) = \min_{t \in [t_0, t_1]} n_i, \quad t_1 = t_0 + \Delta t. \quad (5)$$

and study its heterogeneity. Because free volumes are of a size comparable to σ_1 lasting with a time scale longer than that of thermal fluctuations, the IE average of $\hat{\nu}(\mathbf{r}, \Delta t_b) = \sum_j \nu_j(\Delta t_b) \delta(\mathbf{r} - \mathbf{r}_j(0))$ can illustrate the spatiotemporal heterogeneity of free volumes in an enhanced manner. Figure 5 shows the distribution of 25% of the total number of particles having lower $\langle \nu_i(\Delta t_b) \rangle_{\text{IE}}$ values mapped together with the broken bond distribution $\langle \mathcal{B}_i(\Delta t_b) \rangle_{\text{IE}}$. The lower the value of T is, the more distinct is the correspondence between these distributions. It is noteworthy that for $T = 0.56$, the instantaneous density distribution shown in Fig. 2 exhibits a correlation with that of the free volumes and the broken bonds shown in the figure to the right ($T = 0.56$) in Fig. 5.

Quantitatively, this correspondence is illustrated for $T = 0.56$ in Fig. 6; the correspondence is observed as a scatter plot between $\langle \hat{\nu}(\mathbf{r}, \Delta t_b) \rangle_{\text{IE}}$, with $\hat{\nu}(\mathbf{r}, \Delta t_b) = \sum_j \nu_j \delta(\mathbf{r} - \mathbf{r}_j(0))$ and $\langle \mathcal{B}(\mathbf{r}, \Delta t_b) \rangle_{\text{IE}}$ averaged in each cell, thereby squarely dividing the total system into a 12×12 grid of size $(L/12)^2 = (23.4\sigma_1)^2$, which contains about 440 particles.

To examine how the heterogeneity in the density evolves, in Fig. 7, we show the structure factor of $\hat{\nu}(\mathbf{r}, \Delta t_b)$ defined as

$$S_\nu(k, \Delta t_b) = \langle |\hat{\nu}_{\mathbf{k}}(\Delta t_b)|^2 \rangle_{\text{IE}}, \quad (6)$$

where $\delta \hat{\nu}(\mathbf{r}, \Delta t_b) = \sum_j \sigma_j^2 (\nu_j - [\nu_j]_N) \delta(\mathbf{r} - \mathbf{r}_j(0))$ denotes the mesoscopic fluctuation of ν_i , and $\hat{\nu}_{\mathbf{k}}(\Delta t_b)$ indicates

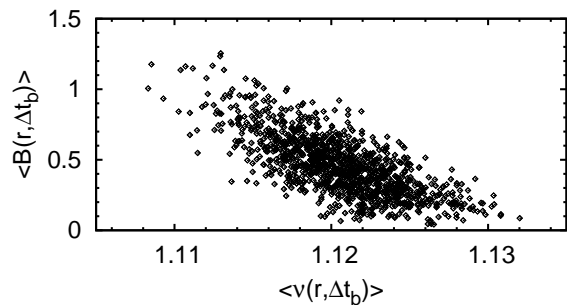


FIG. 6: Scattered plot of cell-averaged quantities between $\langle \hat{\nu}(\mathbf{r}, \Delta t_b) \rangle_{\text{IE}}$ and $\langle \mathcal{B}(\mathbf{r}, \Delta t_b) \rangle_{\text{IE}}$ for $T = 0.56$. The cells divide the total system into a 12×12 grid. The data for runs with eight independent initial conditions are shown in this figure, and an IE average over 32 runs is taken for each run.

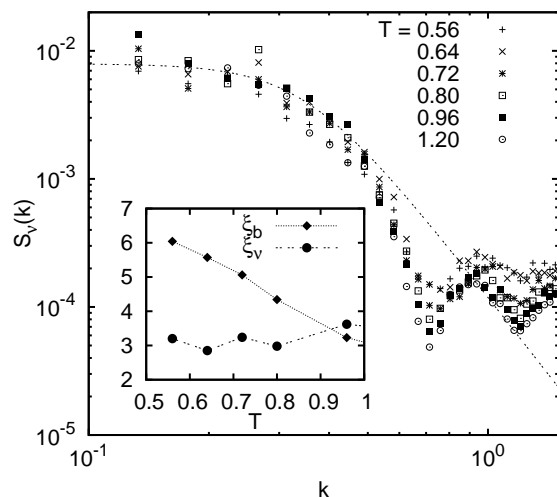


FIG. 7: Structure factor of the minimum local density $S_\nu(k, \Delta t_b)$ defined in Eq. (6). For various values of T , the data are well fitted by $f(k) = C_0(1 + k^4 \xi_b^4)^{-1}$. The dotted line shows the fit at $T = 0.72$. Inset: Correlation lengths of broken bond distribution ξ_b and those of “minimum local density” ξ_ν for various values of T . While the former is estimated by assuming the Ornstein-Zernike form ($\sim (1 + k^2 \xi_b^2)^{-1}$), the latter is plotted by using a sharper form decaying as k^{-4} at $k \sim 0.5$.

the Fourier components of $\delta \hat{\nu}(\mathbf{r}, \Delta t_b)$. The average is taken over IEs of 128 (32 for $T \leq 0.64$) runs generated with 32 independent initial configurations, and thus, data from 4096 (or 1028) runs performed over a duration of Δt_b are used for each T . Since one isolated free volume lowers the values of $n_i(r_0)$ of particles within the distance of $l = r_0 \sigma_1$, we observe a small peak in $S_\nu(k, \Delta t_b)$ around $k \sim 2\pi/l \simeq 10^0$. Remarkably, $S_\nu(k, \Delta t_b)$ is enhanced at low- k , exhibiting the same degree of enhanced heterogeneity. Because the shape of each lower-density region illustrated in Fig. 5 shows sharp boundaries, it is much better fitted with $f(k) = C_0(1 + k^4 \xi_b^4)^{-1}$ than

the Ornstein-Zernike (OZ) form. In the inset of Fig. 7, we compare the correlation lengths ξ_ν and ξ_b of the minimum local density and the broken bond distributions, estimated by fitting $f(k)$ to $S_\nu(k, \Delta t_b)$ and the OZ form to $S_b(k, \Delta t_b)$ (see Refs. 2,3), respectively. For the interval of the corresponding structural relaxation time $\Delta t_b(T)$ the heterogeneity in $\hat{\nu}(\mathbf{r}, \Delta t_b)$ is nearly independent of the temperature, while $S_b(k, \Delta t_b)$ displays the OZ form with growing length scales for lower values of T .

D. Normal mode analysis

Recent numerical simulations evidence that the static particle configuration itself determines the dynamic propensity distribution, even in an amorphous state apparently lacking structural order.^{41,42} In particular, localized soft modes predicted by the “normal mode analysis” have been revealed to be a good predictor of the dynamic heterogeneity; from a single and instantaneous snapshot of the particle configuration, information regarding the spatial heterogeneity of dynamics can be extracted with the use of the distribution of localized low-frequency phonons.^{37,38} Similar methods are also employed to predict yielding spots in a jammed system at zero temperature.^{43,44}

To compare the distribution of the free volumes with the high-propensity region determined from a static configuration, we perform the normal mode analysis for our system along the lines of Ref. 37. After the configuration of the particles $\{\mathbf{r}_i\}$ is quenched to a state with local stability with the use of the conjugate gradient method, the solution $\omega = \omega_k$ of the eigenvalue equation $(D_{i\alpha,j\beta} - \omega^2)a_{j\beta} = 0$ ($\alpha, \beta \in \{x, y\}$) for the $2N \times 2N$ Hessian matrix

$$D_{i\alpha,j\beta} = \frac{1}{\sqrt{m_i m_j}} \left(\frac{\partial^2 V(\mathbf{r})}{\partial \mathbf{r}_i^\alpha \partial \mathbf{r}_j^\beta} \right), \quad (7)$$

is calculated, where i and j denote particle indices. The eigenvalues ω_k and the eigenvectors $\tilde{a}_{j\beta} = a_{j\beta,k}$ represent the frequencies of the normal modes and the amplitudes for k -th mode respectively, the $1 \leq k \leq 2N$ being the mode index. Excluding the two lowest-frequency modes corresponding to the translational motion, we consider the thermal vibration amplitude, *i.e.* the local Debye-Waller factor

$$\mathcal{W}_i = \frac{k_B T}{m_i} \sum_{k=2}^M \frac{a_{ix,k}^2 + a_{iy,k}^2}{\omega_k^2}, \quad (8)$$

where M denotes the number of the lowest-frequency modes taken into account. This quantity represents the strength of the squared vibration amplitude for each particle for small time scales, *i.e.*, localized long-wavelength soft modes represent the propensity distribution. Upon using the equipartition rule, the thermal energy for each mode is given by $k_B T$, which means that we should

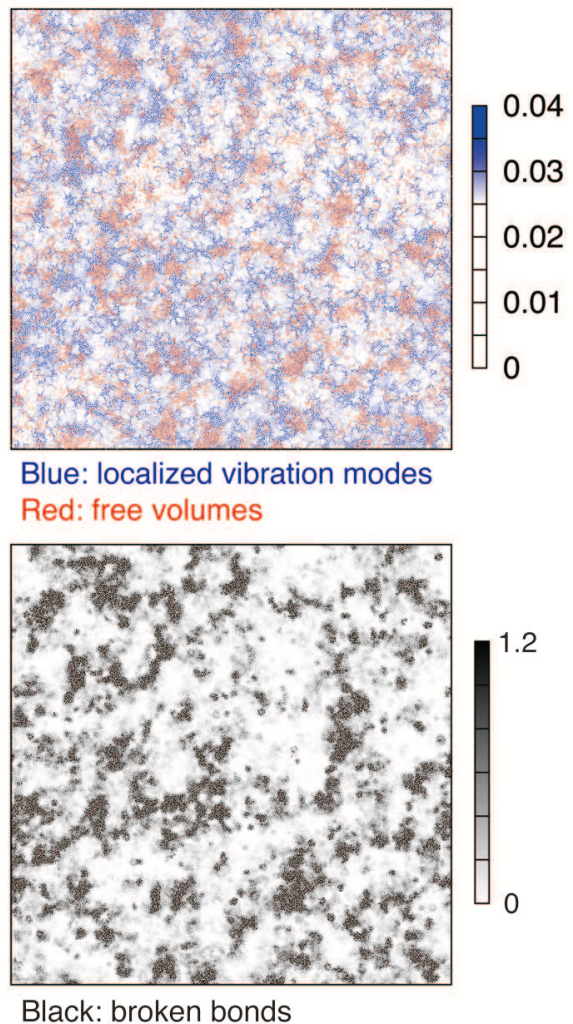


FIG. 8: Top: The local Debye-Waller factor in Eq. (8), where the number of the modes M is 2560, is shown with the blue-colored map for $T = 0.56$ for the same snapshot as in Fig. 5, together with the 25% of the particles having smaller values of $\langle \nu_i(\Delta t_b) \rangle_{\text{IE}}$, *i.e.*, $\langle \nu_i(\Delta t_b) \rangle_{\text{IE}} < 1.11107$. Bottom: The corresponding map of the number distribution of broken bonds for the same IE $\langle \hat{B}(\mathbf{r}, \Delta t) \rangle_{\text{IE}}$ for $T = 0.56$ as in Fig. 5.

weight it by inverse-square frequencies in the superposition of the non-dimensional amplitudes $A_{j\beta,k}$.

In Fig. 8, the spatial distribution of the localized soft modes for $M = 2560$ is shown with the blue-colored map in the top panel, wherein the red particles represent the free volume distribution (the same as those for $T = 0.56$ in Fig. 5). Both the distributions have substantial overlaps with that of broken bonds, as shown separately in the bottom panel of Fig. 8. Free volumes are relatively absent around particles with smaller vibration amplitudes, as represented by blanks in the blue-colored plot. We can also confirm the tendency by measuring the average values over a 24×24 divided mesh, each of which contains about 110 particles. None of the 71 cells having small values of the Debye-Waller factor

($[\mathcal{W}]_{\Sigma} < 0.027$) has the averaged local minimum density $\langle \nu_i(\Delta t_b) \rangle_{\text{IE}} > \nu_0 = 1.11107$, where $[\cdot]_{\Sigma}$ denotes the average over a cell.

While the spacial distribution of the superposition \mathcal{W}_i exhibits localization of the vibration modes, a large-scale heterogeneity can be observed, as observed from Fig. 8. In Fig. 9 (a), the structure factor of \mathcal{W}_i defined by

$$S_{\mathcal{W}}(k) = \langle |\hat{\mathcal{W}}_{\mathbf{k}}|^2 \rangle, \quad (9)$$

where $\hat{\mathcal{W}} = \sum_j \sigma_j^2 \mathcal{W}_i \delta(\mathbf{r} - \mathbf{r}_j(0))$ is shown for various numbers of the lowest-frequency modes $M = 160, 640,$ and 2560 . These data can be fitted well to the OZ form $f(k) = (1 + k^2 \xi_M^2)^{-1}$, where the correlation lengths ξ_M are estimated to be $\xi_M \simeq 7.3 \pm 0.3, 6.3 \pm 0.3,$ and 4.8 ± 0.2 , respectively. On the one hand $S_{\mathcal{W}}(k)$ continues to increase for low values of k for small M ($=160$) because these low normal modes have large scale characteristic lengths, but at the same time it stops growing at low k for $M = 2560$ due to the localization.

To investigate the length scales involved in the correspondence between the heterogeneities presented above, we calculated the coefficients of the spatial correlations of these quantities in the following manner: the system is divided into boxes with lengths $L_d = L/d$ ($d = 2, 3, \dots$). Within each of these boxes, we estimate the average values $[\nu]_{\Sigma}$, $[\mathcal{B}]_{\Sigma}$, and $[\mathcal{W}]_{\Sigma}$, and subsequently, we calculate $\rho_{\mathcal{W}, \mathcal{B}}$ and $\rho_{\nu, \mathcal{B}}$ over d^2 data points, where $\rho_{\alpha, \beta}$ denotes the Pearson correlation coefficients for a pair of statistical data series (denoted by α and β) defined by

$$\rho_{\alpha, \beta} = \frac{\sum (\alpha - E(\alpha)) \cdot \sum (\beta - E(\beta))}{[\sum (\alpha - E(\alpha))^2]^{1/2} [\sum (\beta - E(\beta))^2]^{1/2}}, \quad (10)$$

where $\{\alpha, \beta\} \in \{[\nu]_{\Sigma}, [\mathcal{B}]_{\Sigma}, [\mathcal{W}]_{\Sigma}\}$ and $E(X)$ denotes the average of X over all the boxes. This quantity assumes a value of 1 (or -1) when α and β are perfectly correlated (anticorrelated), and becomes 0 if there are no correlations. In Fig. 9, together with the negative value of $\rho_{\nu, \mathcal{B}}$ representing the anticorrelation between the local density and the broken bonds, $\rho_{\mathcal{W}, \mathcal{B}}$ for $M = 160, 640,$ and 2560 is plotted at various cell sizes L_d whose value corresponds to the degree of coarse-graining. The average is taken over calculations for 16 independent initial configurations. Since the vibrational amplitude \mathcal{W}_i is more directly linked with the short-time vibration motion rather than the broken bond distribution, it has smaller values and larger statistical errors than $-\rho_{\nu, \mathcal{B}}$, but it assumes definitely positive correlations. A noteworthy observation is that, at a large scale ($L_d \sim 100$), the correlation coefficient of \mathcal{W}_i for $M = 160$ with \mathcal{B}_i is as large as that for $M = 2560$. This suggests that the nature of the occurrence of long-range heterogeneity in the dynamics can more or less be described by the long-ranged low-frequency sounds modes, and that the high-frequency modes are relatively irrelevant to the long-ranged dynamical heterogeneity.

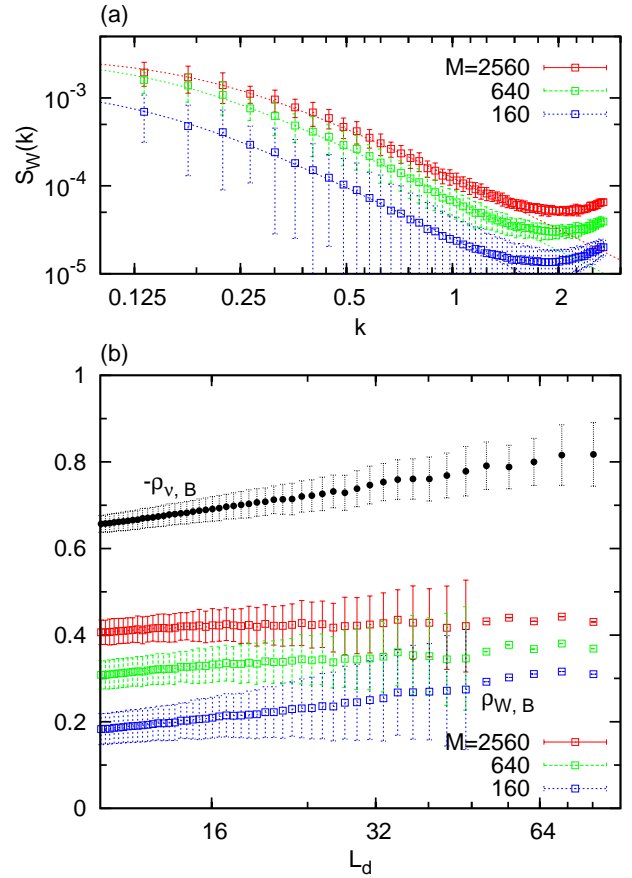


FIG. 9: (a) The structure factor $S_{\mathcal{W}}$ of the thermal vibration amplitude is shown for $M = 160, 640,$ and 2560 lowest eigenfrequencies. Dotted lines represent the fit by the OZ form $f(k) \sim (1 + k^2 \xi_M^2)^{-1}$ for each M . (b) The Pearson correlation coefficients $\rho_{\mathcal{W}, \mathcal{B}}$ for $M = 160, 640,$ and 2560 , and also the minus of $\rho_{\nu, \mathcal{B}}$ are shown for various box cell sizes L_d . The data represent the degree of spatial correlation between \mathcal{W}_i and \mathcal{B}_i . The error bars are abbreviated at large L_d values for the sake of visibility.

IV. CONCLUSION

In this study, the relationship between mesoscopic heterogeneities of free-volume distribution, soft-mode localization, and broken bonds has been investigated. The results show that they are largely correlated with a clear overlap. However, the correlation lengths have qualitatively different characteristics—extensive studies on this topic have revealed that dynamical heterogeneity in a supercooled liquid accompanies largely growing correlation lengths in the dynamics, as is also shown in this study in terms of the parameter ξ_b in Fig. 7. In contrast, the correlation length of the free volume distribution represented by the “minimum local density” does not exhibit growth and remains short-ranged even at a low temperature. Thus, free volumes are distributed over a small range in the regions where configuration rearrangements occur as seeds for dynamic heterogeneity at large lengths

scales. By performing the normal mode analysis, we find that the lowest-frequency $M = 160$ sound modes, which form about 0.1% of the total vibration modes, describes the most of the relationships between the localized soft modes (for $M = 2560$) and the dynamical heterogeneity. Although there is a missing link between the vibrational spectra and broken bond distributions, the data suggest the possibility that large-scale correlation originates from interactions between fragile regions facilitated by large scale sound modes stemming over these regions, and that the free volume is a candidate for the representation of these fragile regions.

Recently, experiments on colloidal clusters^{45,46} and simulations⁹ reveal a correlation between the neighbor number, vibration mode, and irreversible rearrangements. The correlation between the localized vibration modes and the free volumes is attributed to relatively smaller neighbor numbers around the local free volumes, which we speculate as providing collateral evidence for the role of free volume in the heterogeneity. However, the nature of the causal mechanism because of which free volume distributions bring about the long-wavelength sound vibration is still an open question,

We add some remarks for clarification in the following:

(i) The fact that the minimum local density heterogeneity does not depend on the temperature for the same degree of frustration indicates that what we observe as density heterogeneity is not specific to the supercooled state but is inherently present even in simple liquids. Because the configuration changes becomes slower as the system approaches the glass transition, the cooperative motion of free volumes increases at a longer-range to enhance dynamical heterogeneity.

(ii) While in a number of experiments long-ranged correlations of the density in glass have been observed,^{20–24} in the simulation of models with repulsive cores presented in this study, the bare structure factor $S(k)$ does not exhibit growth at long wavelengths, similar to the results of other such studies.^{3,14} Though the possibility of longer-range density correlation is not excluded, it would be weak in a model with a strong frustration. It is also noteworthy that in a single component 2D crystal of Lennard-Jones system, where density fluctuation is enhanced at long-wavelengths, the long-ranged dynamic heterogeneity is brought about by a local diffusion of defects with lower local densities rather than by a long-ranged static

fluctuation,³⁴ in analogy with our current simulation.

(iii) Instantaneous normal modes have been analyzed at a low temperature ($T = 0.56$) as having a large correlation length. No related studies on the analysis of such modes for a system size larger than that used in this study are available; in our study, eigenvectors of a 128000^2 matrix have been calculated. The analysis of localized soft modes indicates that a small number of lowest-frequency soft modes extend over large length scales, endowing the system with long-ranged heterogeneity. In the same model system, large-scale vibration motions throughout the whole system have been observed to be enhanced because the system becomes more and more rigid as we lower the temperature.⁸ These vibrations may possibly facilitate interactions between the far-distance fragile regions, to result in long-range dynamical critical fluctuations. Further studies are necessary to reveal the interplay between the sound modes and the configuration rearrangement.

(iv) Although we have limited ourselves to investigation on the potential role of density fluctuations, it is still an open question what the primary causal reason for the dynamical heterogeneity. The role of other possible static origins that can affect the dynamics, for example, density gradient, bond orientation order, and so on, should be investigated further, which is beyond the current scope of the paper.

Acknowledgments

The authors thank A. Ikeda, K. Miyazaki, A. Onuki, K. Kim, H. Mizuno, Y. Noguchi, and P. Harrowell for enlightening discussions. The numerical calculations were carried out on the SGI Altix ICE 8400EX and NEC SX9 systems at ISSP, University of Tokyo. This work is supported by the Core-to-Core Program “International research network for non-equilibrium dynamics of soft matter” by the Japan Society for Promotion of Science (JSPS), and also partially by a Grant-in-Aid for Scientific Research on Innovative Areas “Synergy of Fluctuation and Structure: Foundation of Universal Laws in Nonequilibrium Systems” (Grant No. 25103010). T. K. was supported by JSPS Research Fellowships for Young Scientists (Grant No. 10J02221).

* Electronic address: shiba@issp.u-tokyo.ac.jp

† Present address: Laboratoire Charles Coulomb, UMR 5221, CNRS and Université Montpellier 2, 34095 Montpellier, France

¹ K. Binder and W. Kob, *Glassy Materials and Disordered Solids* (World Scientific, Singapore, 2005).

² R. Yamamoto and A. Onuki, *J. Phys. Soc. Jpn.* **66**, 2545 (1997).

³ R. Yamamoto and A. Onuki, *Phys. Rev. E* **58**, 3515 (1998).

⁴ T. Muranaka and Y. Hiwatari, *Phys. Rev. E* **51**, R2735 (1995).

⁵ W. Kob, C. Donati, S. J. Plimpton, P. H. Poole, and S. C. Glotzer, *Phys. Rev. Lett.* **79**, 2827 (1997).

⁶ C. Donati, J. F. Douglas, W. Kob, S. J. Plimpton, P. H. Poole, and S. C. Glotzer, *Phys. Rev. Lett.* **80**, 2338 (1998).

⁷ G. Biroli, J.-P. Bouchaud, K. Miyazaki, and D. R. Reichman, *Phys. Rev. Lett.* **97**, 195701 (2006).

⁸ H. Shiba, T. Kawasaki, and A. Onuki, *Phys. Rev. E* **86**,

- 041504 (2012).
- ⁹ T. Kawasaki and A. Onuki, *J. Chem. Phys.* **138**, 12A514 (2013).
 - ¹⁰ K. Kim and S. Saito, *J Chem Phys* **138**, 12A506 (2013).
 - ¹¹ G. Adam and J. H. Gibbs, *J. Chem. Phys.* **43**, 139 (1965).
 - ¹² T. R. Kirkpatrick, D. Thirumalai, and P. G. Wolynes, *Phys. Rev. A* **40**, 1045 (1989).
 - ¹³ T. Kawasaki, T. Araki, and H. Tanaka, *Phys. Rev. Lett.* **99**, 215701 (2007).
 - ¹⁴ H. Tanaka, T. Kawasaki, H. Shintani, and K. Watanabe, *Nature Mater.* **9**, 324 (2010).
 - ¹⁵ M. Dzugasov, S. I. Simdyankin, and F. H. M. Zetterling, *Phys. Rev. Lett.* **89**, 195701 (2002).
 - ¹⁶ M. Leocmach and H. Tanaka, *Nature Commun.* **3**, 974 (2012).
 - ¹⁷ G. S. Matharoo, M. S. G. Razul, and P. H. Poole, *Phys. Rev. E* **74**, 050502(R) (2006).
 - ¹⁸ E. M. Marcotte, F. H. Stillinger, and S. Torquato, *J. Chem. Phys.* **138**, 12A508 (2013).
 - ¹⁹ D. Coslovich, *Phys. Rev. E* **83**, 051505 (2011).
 - ²⁰ E. W. Fischer, G. Meier, T. Rabenau, A. Patkowski, W. Steffen, and W. Thönnies, *J. Non-Cryst. Solids* **131-133**, 134 (1991).
 - ²¹ W. van Meegen and P. N. Pusey, *Phys. Rev. A* **43**, 5429 (1991).
 - ²² T. Kanaya, A. Patkowski, E. W. Fischer, J. Seils, H. Gläser, and K. Kaji, *Acta Polymer.* **45**, 137 (1994).
 - ²³ E. W. Fischer, *Physica A* **201**, 183 (1993).
 - ²⁴ A. Patkowski, T. Thurn-Albrecht, E. Banachowicz, W. Steffen, P. Bösecke, T. Narayanan, and E. W. Fischer, *Phys. Rev. E* **61**, 6909 (2000).
 - ²⁵ M. H. Cohen and D. Turnbull, *J. Chem. Phys.* **31**, 1164 (1959).
 - ²⁶ P. D. Flemming-III and C. Cohen, *Phys. Rev. B* **13**, 500 (1976).
 - ²⁷ A. S. Argon, *Acta Metal.* **27**, 47 (2009).
 - ²⁸ M. D. Ediger, *J. Non-Cryst. Solids* **235-237**, 10 (1998).
 - ²⁹ M. L. Falk and J. S. Langer, *Phys. Rev. E* **57**, 7192 (1998).
 - ³⁰ A. Lemaître, *Phys. Rev. Lett.* **89**, 195503 (2002).
 - ³¹ A. Onuki, A. Furukawa, and A. Minami, *PRAMANA - J. Phys.* **64**, 661 (2005).
 - ³² A. Widmer-Cooper and P. Harrowell, *J. Non-Cryst. Solids* **352**, 5098 (2006).
 - ³³ I. Ladadwa and H. Teichler, *Phys. Rev. E* **73**, 031501 (2006).
 - ³⁴ H. Shiba, A. Onuki, and T. Araki, *EPL* **86**, 66004 (2009).
 - ³⁵ K. Nordlund, Y. Ashkenazy, R. S. Averback, and A. V. Granato, *Europhys. Lett.* **71**, 615 (2005).
 - ³⁶ H. Zhang, M. Khalkhali, Q. Liu, and J. F. Douglas, *J. Chem. Phys.* **138**, 12A538 (2013).
 - ³⁷ A. Widmer-Cooper, H. Perry, P. Harrowell, and D. R. Reichman, *Nature Phys.* **4**, 711 (2008).
 - ³⁸ Y. Matsuoka, H. Mizuno, and R. Yamamoto, *J. Phys. Soc. Jpn.* **81**, 124602 (2012).
 - ³⁹ D. N. Perera, *J. Phys.: Condens. Matter* **10**, 10115 (1998).
 - ⁴⁰ T. Kawasaki and A. Onuki, *Phys. Rev. E* **87**, 012312 (2013).
 - ⁴¹ A. Widmer-Cooper, P. Harrowell, and H. Fynewever, *Phys. Rev. Lett.* **93**, 135701 (2004).
 - ⁴² A. Widmer-Cooper and P. Harrowell, *Phys. Rev. Lett.* **96**, 185701 (2006).
 - ⁴³ K. Chen, W. G. Ellenbroek, Z. Zhang, D. T. N. Chen, P. J. Yunker, S. Henkes, C. Brito, O. Dauchot, W. van Saarloos, A. J. Liu, A. G. Yodh, *Phys. Rev. Lett.* **105**, 025501 (2010).
 - ⁴⁴ M. L. Manning and A. J. Liu, *Phys. Rev. Lett.* **107**, 108302 (2011).
 - ⁴⁵ P. J. Yunker, K. Chen, Z. Zhang, and A. G. Yodh, *Phys. Rev. Lett.* **106**, 225503 (2011).
 - ⁴⁶ P. J. Yunker, Z. Zhang, M. Gratale, K. Chen, and A. G. Yodh, *J. Chem. Phys.* **138**, 12A525 (2013).